metals

MDPI

Article

Interaction of Mechanical Characteristics in Workpiece Subsurface Layers with Drilling Process Energy Characteristics

Michael Storchak [1,2,*], Larysa Hlembotska [2], Oleksandr Melnyk [2] and Nataliia Baranivska [2]

[1] Institute for Machine Tools, University of Stuttgart, Holzgartenstraße 17, 70174 Stuttgart, Germany
[2] Department of Mechanical Engineering, Zhytomyr Polytechnic State University, Chudnivska str. 103, 10005 Zhytomyr, Ukraine; zid_gle@ztu.edu.ua (L.H.); o.l.melnyk@ztu.edu.ua (O.M.); ktpl_bnv@ztu.edu.ua (N.B.)
* Correspondence: michael.storchak@ifw.uni-stuttgart.de; Tel.: +49-711-685-83831

Abstract: The performance properties of various types of parts are predominantly determined by the subsurface layer forming methods of these parts. In this regard, cutting processes, which are the final stage in the manufacturing process of these parts and, of course, their subsurface layers, play a critical role in the formation of the performance properties of these parts. Such cutting processes undoubtedly include the drilling process, the effect of which on the mechanical characteristics of the drill holes subsurface layers is evaluated in this study. This effect was evaluated by analyzing the coincidence of the energy characteristics of the short hole drilling process with the mechanical characteristics of the drilled holes' subsurface layers. The energy characteristics of the short-hole drilling process were the total drilling power and the cutting work in the tertiary cutting zone, which is predominantly responsible for the generation of mechanical characteristics in the subsurface layers. As mechanical characteristics of the drill holes' subsurface layers were used, the microhardness of machined surfaces and total indenter penetration work determined by the instrumented nanoindentation method, as well as maximal indenter penetration depth, were determined by the sclerometry method. Through an analysis of the coincidence between the energy characteristics of the drilling process and the mechanical characteristics of the subsurface layers, patterns of the effect of drilling process modes, drill feed, and cutting speed, which essentially determine these energy characteristics, on the studied mechanical characteristics have been established. At the same time, the increase in the energy characteristics of the short-hole drilling process leads to a decrease in the total indenter penetration work and the maximum indenter penetration depth simultaneously with an increase in the microhardness of the drilled holes' subsurface layers.

Keywords: cutting; short hole drilling; subsurface layers; nanoindentation; sclerometry; indenter penetration work; indenter penetration depth

check for updates

Citation: Storchak, M.; Hlembotska, L.; Melnyk, O.; Baranivska, N. Interaction of Mechanical Characteristics in Workpiece Subsurface Layers with Drilling Process Energy Characteristics. *Metals* **2024**, *14*, 683. https://doi.org/10.3390/met14060683

Academic Editor: Jorge Salguero

Received: 15 April 2024
Revised: 31 May 2024
Accepted: 6 June 2024
Published: 9 June 2024

Copyright: © 2024 by the authors. Licensee MDPI, Basel, Switzerland. This article is an open access article distributed under the terms and conditions of the Creative Commons Attribution (CC BY) license (https://creativecommons.org/licenses/by/4.0/).

1. Introduction

The aspiration to ensure the specified performance properties of critical parts necessitates the search for ways to realize this assurance. One of the possible ways to solve this problem is the application of technological methods, in particular, cutting processes that generate specific subsurface layer mechanical characteristics of parts for various devices and mechanisms in the machining process [1]. These are the characteristics generated by the various cutting processes that are responsible for the sought-performance properties [2]. The relationship between mechanical characteristics and performance properties is particularly significant for critical complex-profile parts [3] functioning in alternating and high contact loads [4]. The mechanical characteristics of the machined subsurface layers of parts that correlate quite closely with various performance properties of these parts include the characteristics of the machined material structure, microhardness of these layers [5], distribution of residual stresses in these layers [6], and the surface integrity of the

machined parts [5,7]. Although each of these mechanical characteristics correlates with the performance properties of machined parts separately, this relationship is unilateral. This transforms into a significant problem when it is necessary to consider the interrelation of multiple mechanical characteristics with performance properties simultaneously. It is especially aggravated when analyzing spatial cutting processes with a significant gradient of tool contact conditions with machined material and gradient of cutting modes, for example, when analyzing one of the oldest machining processes—the drilling process [8]. The use of generalized (integral) mechanical characteristics of subsurface layers is of considerable help in these cases. The characteristics determined by instrumented nanoindentation [9] and sclerometry [10] are used as such characteristics.

The presented study is a continuation of earlier research [11] and its development in terms of investigating the coincidence of mechanical characteristics of holes subsurface layers formed as a result of thermomechanical contact between the tool and the machined material under the conditions of the short hole drilling process.

2. Mechanical Characteristics Determination of Drilled Subsurface Layers

One of the most common and complex cutting processes for various materials is the drilling process [12], occupying 30% to 50% of all cutting processes [13]. In this regard, the drilling process has attracted the attention of many researchers [14]. Along with numerous experimental and theoretical studies of various drilling processes using different types of drills, considerable attention has also been paid to the study of mechanical characteristics of the drill holes subsurface layers [15,16]. These investigations include surface integrity studies [5], which involve studies of the microstructure and microhardness of subsurface layers [7], as well as residual stresses in these layers [6] formed as a result of the drilling process [8].

The influence of contact conditions and peculiarities of the drilling process with the insertion of additional energy in the form of vibrations on the surface integrity, in particular on the plastic degree deformation of the machined material, its microhardness distribution, the magnitude of residual stresses and others is the subject of a study by Sun and colleagues [17]. Strodick et al. studied the effect of cutting modes on surface integrity during deep-hole drilling with BTA drills [18]. The focus of Ren and Liu's study was the effect of cutting modes on the work hardening of machined material [19]. The study results of the residual hole surface roughness dependence on cutting modes during the drilling of AISI H11 tool steel are presented in the work of Garg and Goyal [20]. Studies by Lacombe and colleagues proved the significant influence of microhardness, as one of the characteristics of drilled hole surface integrity, on the fatigue strengths of aluminum alloy parts [21]. The authors of the study also noted significant dependence of such characteristics of drill hole surface integrity as machined surface roughness, microhardness, and microstructure of machined subsurface layers on cutting modes [22].

Recently, researchers have also been attracted to the study of surface integrity characteristics of the surface machined by drilling various heterogeneous materials, mainly composite materials. In addition to the accepted surface integrity characteristics, such studies also consider the delamination processes of composite materials [23], dislocation development [24], and dislocation degree [25] of the mentioned composite materials. A significant number of publications are devoted to the study of surface integrity characteristics of holes during the drilling of difficult-to-machine materials, such as titanium alloys and nickel-containing alloys. In the study of titanium alloy drilling, the alloy Ti-6Al-4V was generally used as the machined material. While analyzing the microstructure of the hole subsurface layers during the drilling of titanium alloy Ti-6Al-4V, Varote and Joshi found a relationship between such characteristics of the microstructure as grain size and disorientation angle with drilling modes and the presence of lubricating and cooling fluids [26]. Similar studies were carried out by Haddag et al. [27], using the analysis of the microhardness distribution of subsurface layers to estimate the microstructure of these layers. Wang and colleagues related the microstructure of subsurface layers to their micro-

hardness and residual stress distribution in these layers [28]. A significant part of studies on the drilling process of titanium alloys is devoted to the dependence evaluation of the roughness geometric parameters of drilled holes on the cutting process conditions, particularly the drill feed and cutting speed [29,30]. Considerable attention is also paid to the analysis of microhardness of cutting machined subsurface layers of titanium alloys during drilling [31,32], the influence of various lubricating and cooling fluids and methods of their supply to the cutting zone on the formation of surface integrity characteristics [33], the analysis of the influence of special geometrical parameters of drills on surface integrity [34], and others.

In the study of the surface integrity of drilled holes in nickel-containing alloys, Inconel 718 alloy served as a prime example of the machined material. Lotfi et al. evaluated the relationship of drilling conditions of Inconel 718 alloy, in particular, drill feed and the drill revolutions number, with the microhardness of holes subsurface layers, microstructure, and roughness height parameters [35]. They analyzed the influence of the cutting modes noted above on the microstructure characteristics using a numerical drilling model. A study of the drilling process conditions effect of nickel alloy UDIMET 720 on the surface topography of drill holes' subsurface layers and microhardness is presented in research by Dutilh and colleagues [36]. The influence of tool geometric parameters on the structure of Inconel 718 alloy was evaluated in a study by Xu and colleagues [37]. The study by Rahim and Sasahara [38] concentrated on analyzing the effect of the coolant delivery method and its composition on surface integrity characteristics such as microhardness of subsurface layers, surface roughness of drill holes subsurface layers, and plastic deformation of subsurface layers in the machined Inconel 718 alloy. Karabulut and Kaynak showed the possibilities of improving the machined surface quality compared to the drilled surface in the same deformed alloy by studying the drilling process of additively manufactured Inconel 718 alloy [39]. Its height roughness parameters were used to evaluate the surface quality.

The residual stress distribution in subsurface layers due to the cutting process and the significant influence of this surface integrity characteristic on the fatigue resistance of machined parts is of particular interest to researchers. The methodological peculiarities of determining residual stresses in the holes' subsurface layers formed during drilling were studied by Girinon and colleagues [40]. Nobre and Outeiro developed an experimental and numerical method to estimate the residual stresses in the subsurface layers of the workpiece formed by the drilling process [41]. An analytical model for calculating residual stresses in subsurface layers induced by the drilling process was developed by Rasti and coworkers [42]. The developed model was based on the analytical model of orthogonal cutting, equivalently transformed to the conditions of the main cutting edge of the drill. Experimental values of residual stresses determined by instrumented nanoindentation were used to validate the proposed model. A numerical spatial model to simulate the residual stresses generated by the reaming process is proposed by Leveille et al. [43]. Experimentally measured cutting forces were used as boundary values of the kinetic characteristics of the reaming process. Wu and colleagues investigated the distribution of residual stresses formed in the subsurface layers of aluminum alloy sheets due to the drilling process [44]. To reduce the residual stress magnitudes, the fastening parameters of the sheet material are optimized.

The characteristics of surface integrity that are considered as a result of the drilling process on various structural materials are ambiguous and often contradictorily related to the cutting process conditions. To clarify this relationship and attempt to ensure its unambiguity, generalized (integral) mechanical characteristics of subsurface layers [11] determined by instrumented nanoindentation [45,46] and sclerometry [47,48] have recently been used. The state-of-the-art instrumented nanoindentation method [49] was developed based on the research of Atkins and Tabor [50]. Later, this method was significantly modified by creating new algorithms for analyzing test results [51] and devices for its implementation [52]. The indenter surface scratching test method, called sclerometry, was created mainly for the analysis of various coatings [53], particularly for the evaluation of the retention strength of the coating on the substrate surface [54] and the adhesion ability

of coatings [55]. Subsequently, a multi-pass sclerometry method [56,57] was proposed to reduce the uncertainty in estimating the pavement failure load [58]. Significant researchers' attention has also been directed towards the development of new devices to realize instrumented nanoindentation [59,60] and sclerometry [61], as well as improvements to existing devices [62,63]. Besides the modernization of the mechanical and electrical parts of the devices for the realization of the specified test methods, the main direction of development and research of the devices was the development of testing methodology. Research on improving instrument calibration methods [64], as well as methods for determining and evaluating measurable mechanical properties [65,66], fully relate to this.

The instrumented nanoindentation method was mainly used to determine the same surface integrity characteristics discussed above: microhardness of the subsurface layers, strain degree of the machined material, material microstructure parameters, and residual stresses in the subsurface layers. Using the instrumented nanoindentation method of five different materials in terms of deformability, Tsybenko et al. evaluated the microhardness of pre-applied scratches and the effect of test conditions on this microhardness [67]. England et al. investigated the relationship between microhardness and corrosion resistance of AM 316L steel [68]. The influence of microhardness determined using instrumented nanoindentation on precipitation strengthening of steels with different alloying is studied by Moon et al. [69].

Li and colleagues used the instrumented nanoindentation method to obtain flow curves of AISI 1045 steel [70]. Through instrumented nanoindentation, Paul et al. [71] investigated the possibility of evaluating the deformation capacity and fracture behavior of 304L steel by nanoindentation. The mechanical properties of 18CrNiMo7-6 steel were determined via instrumented nanoindentation by Zhou and his colleagues [72]. The instrumented nanoindentation method has also been successfully used to determine residual stresses in various materials, such as copper foil [73], films and coatings [74], austenitic steels [75], and other difficult-to-machine steels and alloys. The study of microstructure and mechanical properties of various materials has also been successfully performed using the sclerometry method. Fan et al. investigated the nanomechanical properties of newly synthesized high entropy alloys [76] using the sclerometry method. The effect of sclerometric modes on the mechanical properties of subsurface layers of Ti-6Al-4V titanium alloy was the focus of a study by Pratap and colleagues [77].

In addition to determining the above-mentioned individual surface integrity characteristics, the instrumental nanoindentation method and the sclerometry method are also used to determine the energetic (integral) mechanical characteristics of the subsurface layers [11,78]. Bezyazychnyy et al. investigated the influence of cutting modes, in particular cutting speed and tool feed, during the turning of chrome-nickel alloy on the accumulated strain energy of the workpiece subsurface layers [79]. The relationship between the microhardness of subsurface layers of various steels and alloys and the strain energy of the machined material was studied by Yamamoto et al. [80]. Ren and Liu [19] have established a relationship between the work hardening of Inconel 718 alloy and the turning conditions of this machined material.

Thus, the analysis of known methods leads to the conclusion that the instrumented nanoindentation method and the sclerometry method can also be used to determine the mechanical characteristics of the hole subsurface layers formed due to the drilling process.

3. Materials and Methods

The formation patterns of physical and mechanical characteristics of the workpiece subsurface layers during real spatial cutting processes, such as, for example, turning, drilling, milling, threading, and others, are of the greatest interest due to the widespread use of these cutting processes in production. This study aims to establish the relationship between the energy characteristics of the short hole drilling process and the mechanical characteristics of the hole subsurface layers formed during the drilling process. This will ensure that the desired mechanical characteristics are subsequently generated by setting the

appropriate energy characteristics of the drilling process. The paper studies the formation patterns of mechanical characteristics of subsurface layers in one of the most common cutting processes—the drilling process. The mechanical characteristics study of the hole subsurface layers formed during short hole drilling is a continuation and methodological extension of the previously published study [11] devoted to the orthogonal cutting process. The flowchart of information data flow, which is a methodology for studying the coincidence of mechanical characteristics of subsurface layers formed in the drilling process with the integral characteristics of the cutting process, is presented in Figure 1.

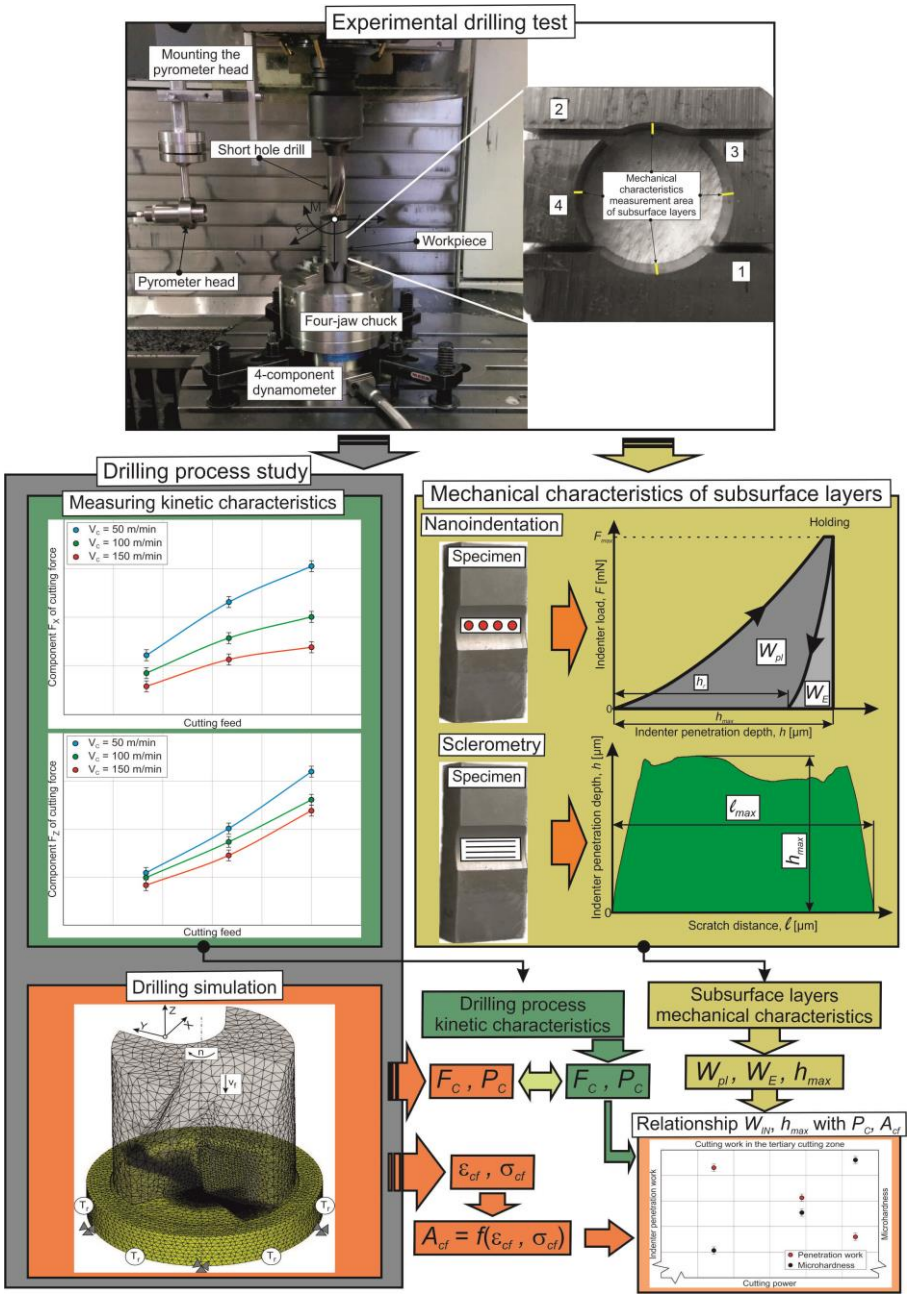

Figure 1. Methodology scheme for determination of physical and mechanical characteristics of drilled subsurface layers.

The experimental studies are divided into two parts: measurement of cutting forces during short hole drilling and determination of mechanical characteristics of drill hole subsurface layers using instrumented indentation and sclerometry. This step is performed as the initial step. The measured components of the cutting forces are used to determine

the cutting power P_C. In parallel, the microhardness of the subsurface layers and the total work of indenter penetration W_{IN}, as well as the maximum depth of indenter penetration h_{max} during sclerometry, are determined from the diagrams of indenter penetration into the specimens' machined surface. These studies are performed in the second step. The third step of the study is devoted to determining the cutting work when drilling short holes in the tertiary cutting zone A_{dcf}. Since the determination of cutting work in the specified zone experimentally causes significant difficulties for real spatial cutting processes, in particular drilling, this characteristic is determined using a numerical cutting model. In the last fourth step of the research methodology, the coincidence of the mechanical characteristics of the subsurface layers formed by the short hole drilling process with the integral characteristics of the cutting process (P_C and A_{dcf}) is identified. This is the focus of the entire study.

3.1. Materials

The machining of the test material by short hole drilling was carried out at the machining center UWF 1202 H (Hermle AG, Gosheim, Germany) (see Figure 1, top, left). The well-known AISI 1045 structural steel was used as the machined material. Table 1 summarizes the mechanical and thermal properties of the machined material. The characterization of the experimental setup, the measuring circuit for determining the components of the cutting force, the used tool (a short hole drill equipped with two carbide inserts: outer and inner) and its geometrical parameters, as well as the initial geometry of the machined workpiece, are given in a previously published study [81].

Table 1. Mechanical and thermal properties of the steel AISI 1045 and carbide inserts adapted from Refs. [82,83].

Material	Strength (MPa)		Elastic Modulus (GPa)	Elongation (%)	Hard-ness	Poisson's Ratio	Specific Heat (J/kg·K)	Thermal Expansion (μm/m·°C)	Thermal Conductivity (W/m·K)
	Tensile	Yield							
AISI 1045	690	620	206	12	HB 180	0.29	486	14	49.8

To determine the resulting cutting force F_C when drilling short holes, the three components F_x, F_y, and F_z were measured (see Figure 1, top left). The feed motion during machining was carried out by displacement of the table with the workpiece fixed on a 4-component dynamometer to the drill fixed in the spindle of the machining center. The feed was varied at three levels: 0.05 mm/rev, 0.1 mm/rev, and 0.15 mm/rev. The nominal cutting speed was also varied at three levels: 50 m/min, 100 m/min, and 150 m/min. To achieve reliability of measurements, the drilling process was repeated at least five times for each set of cutting modes. The maximum error in measuring the cutting force components did not exceed 11%.

The mechanical characteristics of the subsurface layers generated during the short hole drilling process were determined using instrumental nanoindentation and sclerometry. The specimens for measuring mechanical characteristics were prepared from drilled workpieces cut into separate parts (see Figure 1, top, right). Schemes for measuring mechanical performance are illustrated in Figure 2. The Fischer Picodentor HM500 (Helmut Fischer Ltd. Institute for Electronics and Measurement Technology, Sindelfingen, Germany) measuring system was used to perform experimental studies using the instrumental indentation method [11,57]. The instrumented indentation was carried out on the specimen hole surfaces drilled at different cutting speeds and tool feeds. Berkovich indenter was used for measurements. The maximum force on the indenter was 450 mN. The measurement accuracy of the indenter applied load was 0.02 mN. The change of indenter load rate was 20 mN/s. After reaching the maximum load on the indenter during the test, a hold at the specified load for 5 s was performed (see Figure 2a). The measurement accuracy of the indenter penetration depth into the test specimen was 5 nm. Tests of the drilled specimen with each set of cutting speeds and drill feeds were repeated at least 10 times. The processing results of each obtained indenter penetration diagram were the Vickers microhardness of the drilled hole subsurface layers and the total work of indenter penetration W_{IN} (see the

diagram in Figure 2a). The processing results of loading diagrams were averaged for each set of cutting speeds and drill feeds. The largest error in measurement in the diagrams' results processing did not exceed 10%.

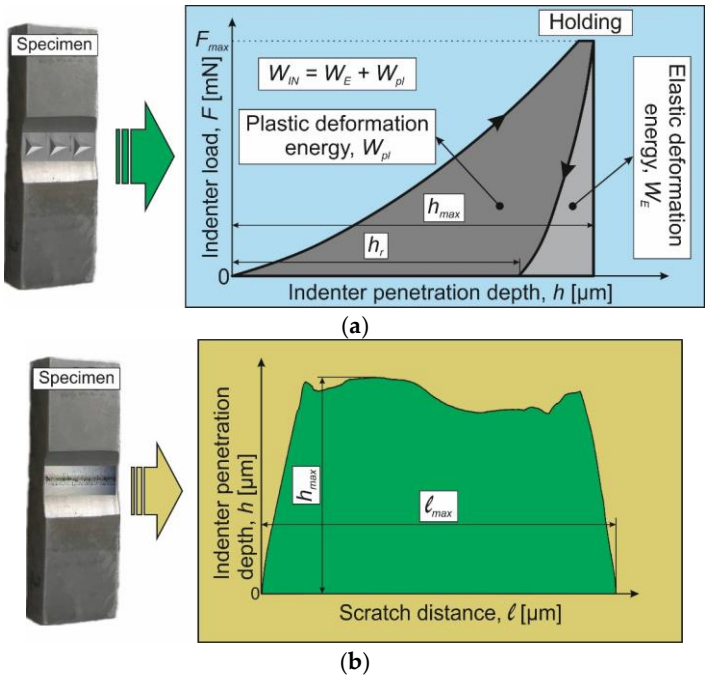

Figure 2. Schematics for mechanical characteristics measurement: (**a**) measurement scheme for instrumented nanoindentation; (**b**) measurement scheme for sclerometry.

Studies of subsurface layers' mechanical characteristics of drilled holes by the sclerometry method were carried out using the device "Micron-gamma" [11,57]. To carry out the studies noted above, a Berkovich indenter was installed so that the projection of one of its edges was parallel to the vector of the indenter movement velocity. The load on the indenter during sclerometry was 100 mN, its movement speed was 20 μm/s, and the length of the produced scratch was 630 μm. The test diagram (sclerogram) determined the maximum depth of indenter penetration along the length of the produced scratch (see the diagram in Figure 2b). Sclerometric tests of the drilled specimen with each set of cutting speeds and drill feeds were repeated at least 10 times. The error in determining the maximum indenter penetration depth resulting from sclerometry did not exceed 11%. The produced scratches were analyzed visually using an optical profilometer, "Micron-alpha" (Micron Ltd., Kyiv, Ukraine) [11,57]. The image vertical resolution provided by the device "Micron-alpha" was 2 nm.

3.2. Methods

The short hole drilling process is a prime example of a real cutting process. In the cutting zones of this machining process, a three-dimensional stress-strain state of the machined material is realized [84]. Under such loading conditions, either adiabatic hardening of the machined material or isothermal softening of this material is realized in the cutting zones [83,85]. Under such loading conditions of the machined material during drilling, the corresponding mechanical characteristics of the subsurface layers are generated. Thus, the patterns of these mechanical characteristic's generation are essentially formed by the loading conditions of the machined material, which, in turn, are determined by the cutting process characteristics. Following the analogy with the first part of the study of the mechanical properties' formation of the machined subsurface layers [11], the total drilling power P_C and the drilling work in the tertiary cutting zone A_{dcf} was chosen as the characteristics determining the loading conditions of the machined material in the drilling process. Fol-

lowing the study methodology, the coincidence of the mentioned integral characteristics of the drilling process with the generated mechanical characteristics of the holes' subsurface layers formed during the short hole drilling process will be identified.

The following relationship is used to determine the total drilling power P_C [84,86]:

$$P_C = F_C \cdot V_C, \quad (1)$$

where F_C—is the resultant cutting force, V_C—is the cutting speed.

The deformation work of the machined material in the tertiary cutting zone A_{dcf} was determined in the dependence of equivalent stresses σ_{dcf} acting in the tertiary cutting zone of the machined material and strains ε_{dcf} of the machined material in this zone:

$$A_{dcf} = V_m \cdot \int_{t_s}^{t_e} \sigma_{dcf} d\varepsilon_{dcf}, \quad (2)$$

where V_m is the material removal volume, t_s and t_e are the simulation start and end times, respectively.

Determination of the deformation work of the machined material in the tertiary cutting zone during short hole drilling was performed using the previously developed numerical cutting model of the drilling process [81]. According to the developed finite element model of the short hole drilling process, the workpiece material was modeled as an isotropic material and the drill as an ideally rigid body [87]. The behavior of the machined material under thermomechanical loading during cutting was described by the Johnson-Cook constitutive equation [88,89].

The Columbian friction model was used to describe the contact interaction conditions between the drill and the machined material [90]. The friction coefficient values in different cutting zones and their areas were determined according to the previously developed methodology [91]. An algorithm embedded in the software [92] was used to separate machined material into the volume of the chip and machined workpiece body. In this regard, it was not necessary to apply a special fracture model of the machined material [93]. Determination of equivalent stresses in the tertiary cutting zone of machined material and material deformations in the process of drilling short holes were performed using tracking points. The layout of the tracking points is shown in Figure 3.

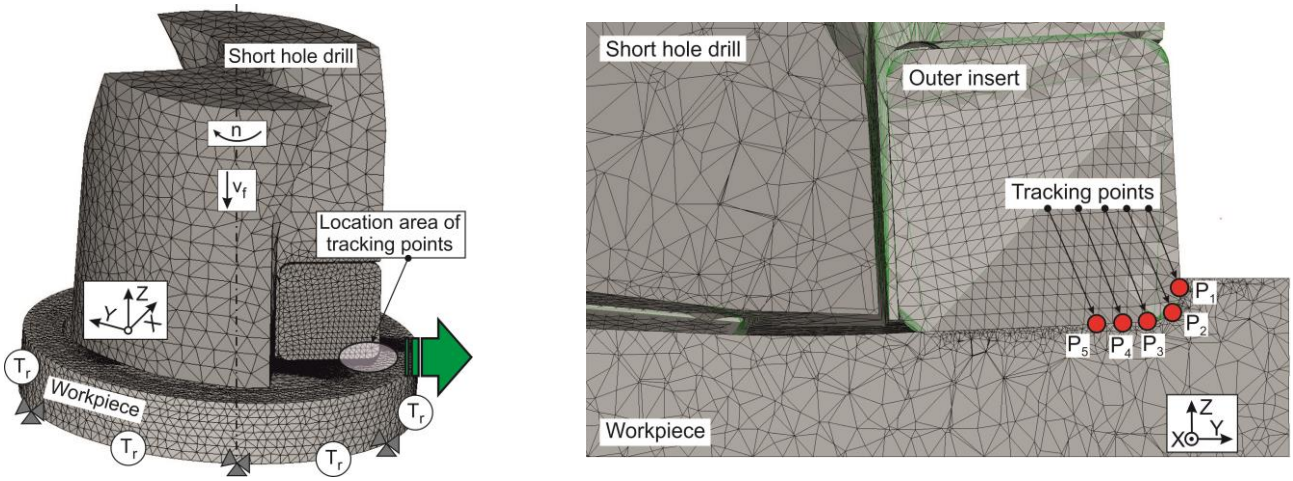

Figure 3. Layout scheme of tracking points: (**a**) initial geometric model of milling with a mesh and boundary conditions; (**b**) location of tracking points.

Five tracking points (P_1, P_2, P_3, P_4, and P_5) were used to determine the drill work, as shown in Figure 3b. The equivalent stresses and strains of the machined material were averaged over the specified five tracking points.

4. Results

As noted in Section 3.2, the integral characteristics of the cutting process are used to evaluate the effect of the short hole drilling process on the mechanical characteristics of the drill hole subsurface layers. The total drilling power P_C and the cutting work in the tertiary cutting zone A_{dcf} are chosen as such characteristics. The total drilling power P_C was determined using the resultant cutting force F_C (see Equation (1)). Figure 4 shows the effect of drill feed on the resultant cutting force and cutting power at different cutting speeds. The resulting cutting force F_C increases monotonically with increasing drill feed f. At the same time, the increase in cutting speed has a somewhat opposite effect: the increase in cutting speed V_C causes a decrease in the resultant cutting force (see Figure 4a). Increasing the drill feed leads to a significantly greater increase in the total cutting power than in the resultant cutting force (see Figure 4b). An increase in cutting speed causes a proportional increase in cutting power.

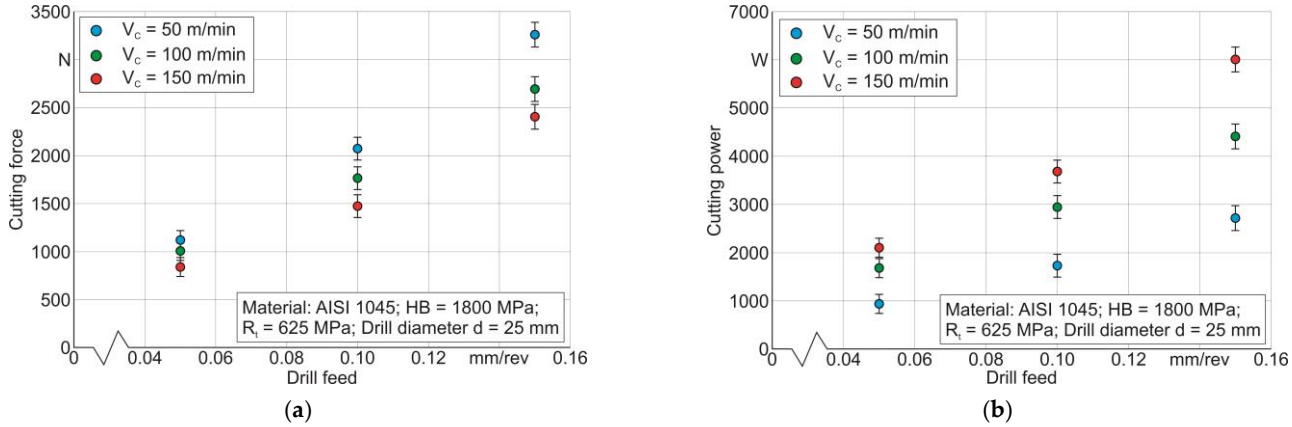

(**a**) (**b**)

Figure 4. Dependence of the resultant cutting force and cutting power on drill feed and cutting speed: (**a**) cutting modes influence on the resultant cutting force; (**b**) cutting modes influence on cutting power.

To determine the cutting work in the tertiary cutting zone A_{dcf}, the simulated values of equivalent stresses σ_{dcf} and corresponding strains ε_{dcf} of the machined material in the specified cutting zone are used. The stresses and strains required for this calculation are simulated using a numerical drilling model (see Section 3.2). To prove the valid simulation of equivalent stresses and strains, the adequacy of the previously developed finite element drilling model [81] was verified. The adequacy of the drilling model was tested by comparing experimentally determined and simulated values of the resultant cutting force and total drilling power. The results of this comparison are presented in Figure 5. The deviation of the experimentally determined resultant cutting force from its simulated value at cutting speed V_C = 50 m/min ranges from 10.6% to 18.2% for the corresponding drill feed variation from 0.05 mm/rev to 0.15 mm/rev (see Figure 5a). The deviation between the experimentally determined and simulated values of the resulting cutting force at cutting speed V_C = 100 m/min ranges from 12.1% to 22.7% for the corresponding drill feed variation from 0.05 mm/rev to 0.15 mm/rev (see Figure 5b). The specified deviations of the resulting cutting force at a cutting speed of V_C = 150 m/min range from 18.6% to 26% for the corresponding drill feed variation from 0.05 mm/rev to 0.15 mm/rev (see Figure 5c). The same deviations were determined between the simulated and experimentally determined values of the total drilling power (see Figure 5d–f). Since the deviations between the experimental and simulated values of the specified drilling process characteristics range from 10.6% to 26%, it can be stated that the finite element drilling model can be used to

simulate equivalent stresses and corresponding strains of machined material in the tertiary cutting zone.

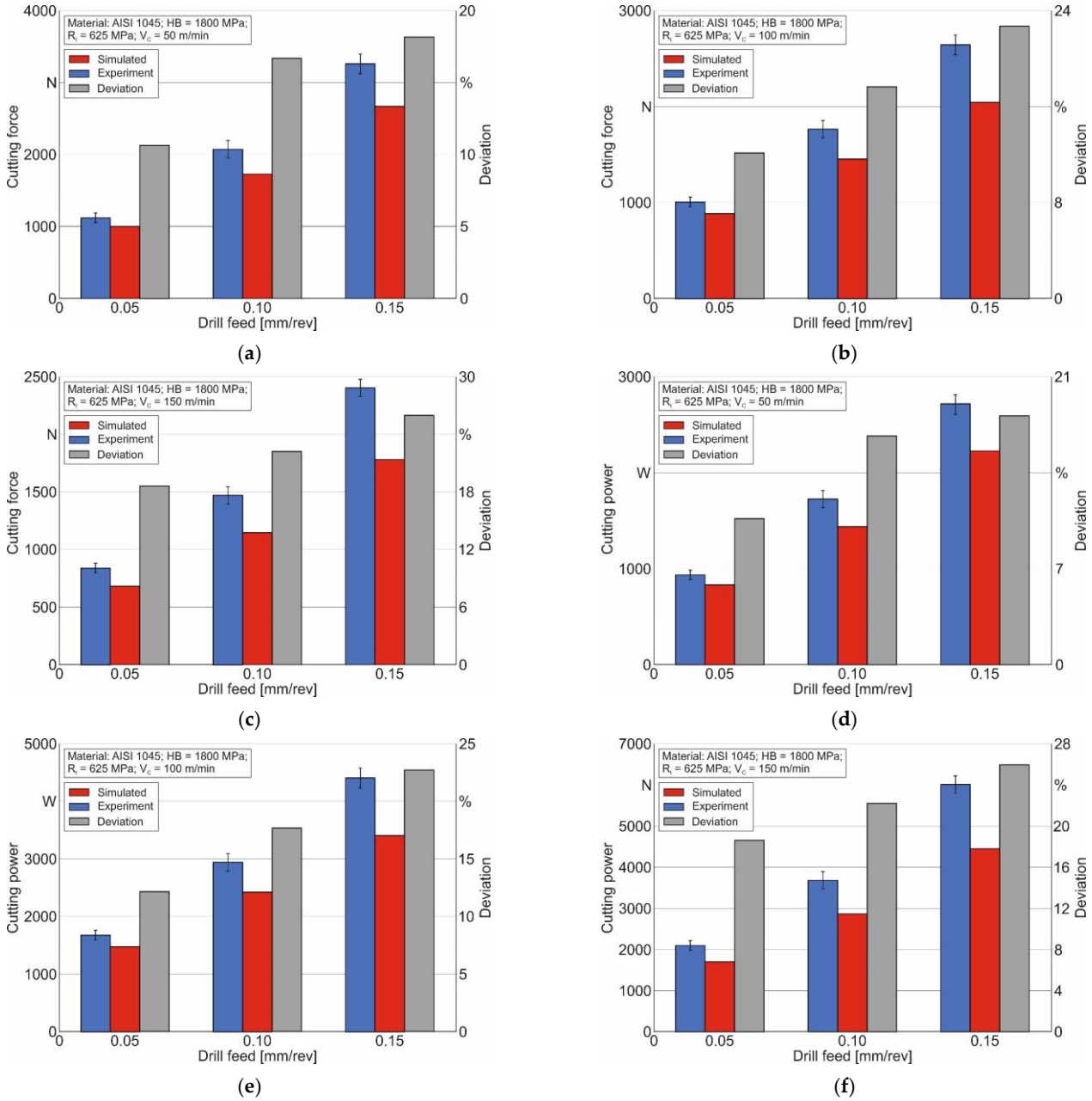

Figure 5. Experimental and simulated values comparison of the resultant cutting force and cutting power at changing of the cutting modes: (**a**) cutting force dependence on drill feed at cutting speed V_C = 50 m/min; (**b**) cutting force dependence on drill feed at cutting speed V_C = 100 m/min; (**c**) cutting force dependence on drill feed at cutting speed V_C = 150 m/min; (**d**) cutting power dependence on drill feed at cutting speed V_C = 50 m/min; (**e**) cutting power dependence on drill feed at cutting speed V_C = 100 m/min; (**f**) cutting power dependence on drill feed at cutting speed V_C = 150 m/min.

The relationship between the simulated values of equivalent stresses and strains of machined material in the tertiary cutting zone determined for five tracking points, for a cutting speed of V_C = 100 m/min and a feed f = of 0.1 mm/rev, is shown in Figure 6a. Figure 6b illustrates the simulated value of the dependence of cutting work on the drill

feed for different cutting speeds. Cutting work A_{dcf} increases in proportion to the increase in drill feed and also grows with rising cutting speed.

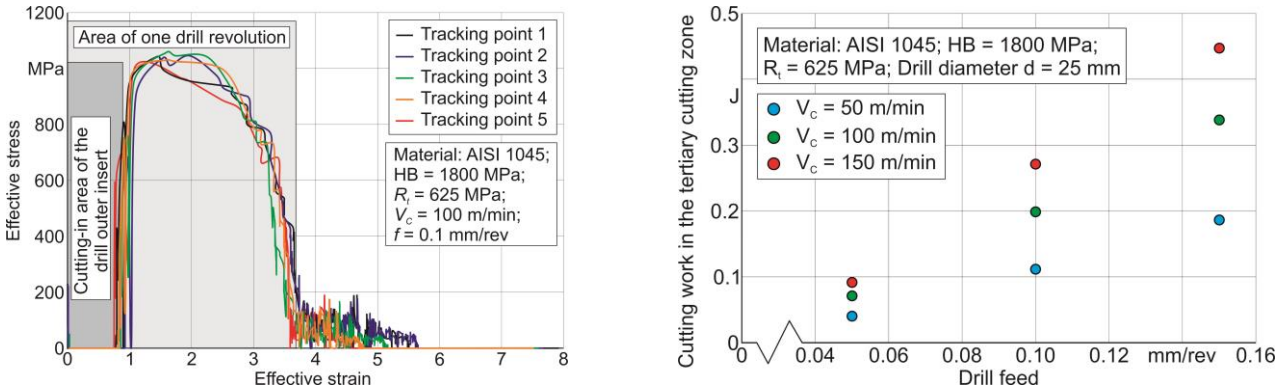

Figure 6. Cutting work A_{cf} in the region of the tertiary cutting zone: (**a**) relationship between effective stress and effective strain for five tracking points; (**b**) effect of drill feed and cutting speed on cutting work A_{cf}.

Following the study methodology (see Section 3, Figure 1), the microhardness and total indentation work, as well as the maximum indentation depth, were considered as the mechanical characteristics of drilled hole subsurface layers. The microhardness and the total indenter penetration work were determined using the instrumented nanoindentation method. The maximal indenter penetration depth was studied using sclerometry (see Section 3.1). The study results of the mechanical characteristics noted above using the instrumented nanoindentation method and a drill feed for different values of cutting speed are presented in Figure 7. The microhardness of the drill hole subsurface layers increases in proportion to the drill feed, as shown in Figure 7a. At the same time, as the cutting speed increases, the microhardness of machined material subsurface layers decreases. Increasing the drill feed leads to a monotonic lowering of the total indenter penetration work W_{IN}, as shown in Figure 7b. Conversely, an increase in cutting speed leads to an increase in work W_{IN}.

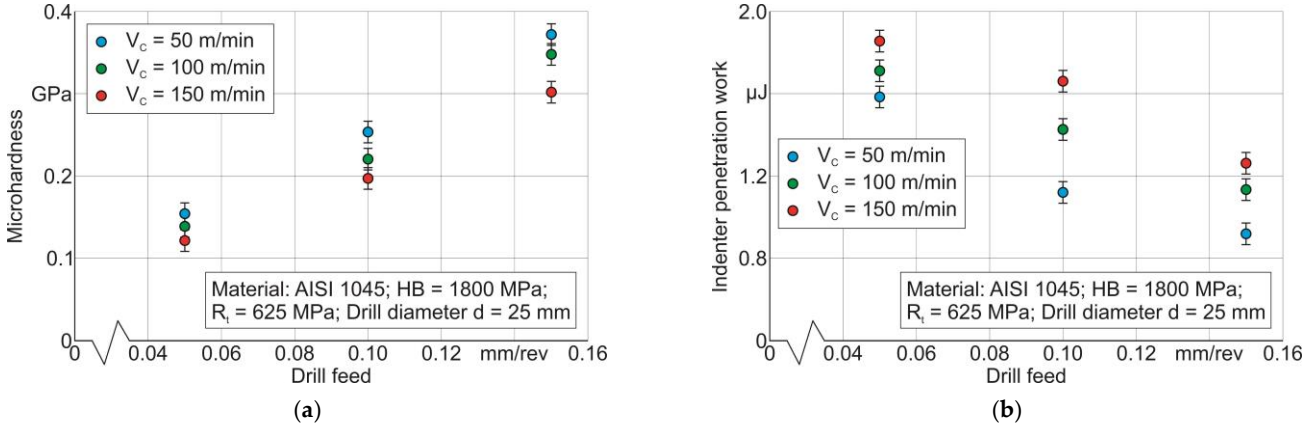

Figure 7. Effect of drill feed and cutting speed on microhardness of drill hole subsurface layers and total indenter penetration work: (**a**) microhardness dependence on cutting modes; (**b**) indenter penetration work dependence on cutting modes.

Cutting modes have a similar effect on the maximum indenter penetration depth h_{max} during sclerometry: with increasing drill feed, the depth h_{max} monotonically decreases, and with increasing cutting speed, the maximum indenter penetration depth increases—Figure 8.

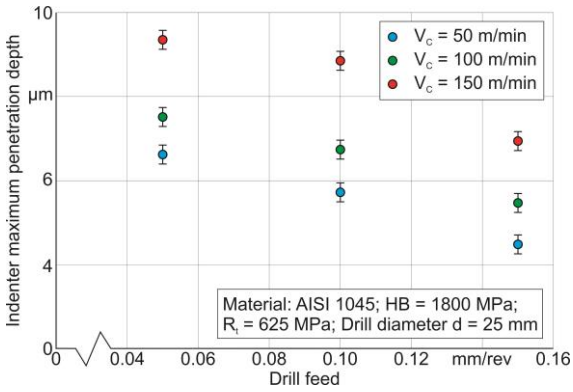

Figure 8. The indenter penetration depth depends on the cutter feed.

5. Discussion

The process of short hole drilling is evident to the external environment, including an outside observer, by various phenomena and characteristics similar to other types of spatial cutting processes. The most sensitive and informative characteristics of the drilling process, which have a significant impact on the mechanical characteristics of cutting machined subsurface layers, are the integral, mainly energy characteristics of this process: total cutting power and cutting work in the tertiary cutting zone. These characteristics of the drilling process are significantly dependent on the cutting modes, in this case, the drill feed and cutting speed. This is shown by the experimental studies presented in Figure 4. The rise in cutting power with increasing drill feed is due to the proportional increase in the volume of machined material removed during the cutting process (see Figure 4a) [84,86]. The decrease in total cutting power with increasing cutting speed is due to the softening of the machined material resulting from a significant increase in cutting temperature [94] due to the increase in cutting speed [95,96]. The same influence mechanisms underlie the variation patterns of cutting work in the tertiary cutting zone as a function of changes in drill feed and cutting speed (see Figure 4b).

Cutting modes in the short hole drilling process logically also have a significant effect on the mechanical characteristics of the subsurface layers since changes in cutting modes, in particular, drill feed and cutting speed, entail significant changes in the thermomechanical effect of the drill on the machined material [95,96]. In turn, the growth of plastic strain causes hardening of the subsurface layers of machined material and, as a consequence, an increase in the microhardness of the machined subsurface layers (see Figure 7a). An increase in cutting speed has the opposite effect on the microhardness of the subsurface layers due to the softening of the machined material resulting from an increase in cutting temperature [84,86] caused by an increase in cutting speed [94]. The considered effect mechanisms of drill feed and cutting speed changes on the state of machined subsurface layers have the opposite effect on the total indenter penetration work W_{IN} (see Figure 7b). This can be explained by the fact that the work W_{IN} decreases with the hardening of the test material and increases with its softening. The effect of cutting modes on the maximum indenter penetration depth h_{max} during sclerometry can also be interpreted similarly (see Figure 8).

The influence of cutting modes on the mechanical characteristics of drill holes' subsurface layers is simplistic and mechanistic since they do not identify the physical sense of the cutting process's impact on these mechanical characteristics. The main factors determining the process of generating mechanical characteristics of subsurface layers as a result of the thermomechanical impact of the drill on the machined material are the hardening and softening processes of subsurface layers [95,96]. Cutting modes, in particular drill feed and cutting speed, influence the hardening or softening of the machined material. However, there is only a correlation between these cutting modes and the mechanical characteristics of the machined subsurface layers. At the same time, there is a lack of possibility to predict

which processes—hardening or softening of the machined material—will prevail at which values of cutting modes.

Consequently, there is an absence of the possibility of changing the mechanical characteristics of the machined subsurface layers using a targeted approach. This possibility is available from the integral (energy) characteristics of the cutting process, particularly the characteristics discussed above: the total drilling power and the cutting work in the tertiary cutting zone. This is explained by the fact that the energy characteristics of the cutting process fully numerically reflect the effects of the thermomechanical impact of the tool on the machined material, determining the prevalence of either kinetic impact [85,86] or thermal impact [94,97].

Following the above-mentioned, the coincidence between the mechanical characteristics of the drill holes' subsurface layers and the energy characteristics of the drilling process was analyzed. Figure 9 shows the coincidence results of indenter penetration work with microhardness and total cutting power, as well as cutting work in the tertiary cutting zone at different drill feeds. The specified coincidence of mechanical characteristics and energy characteristics of the drilling process at a drill feed of f = 0.05 mm/rev is shown in Figure 9a, at a drill feed of f = 0.1 mm/rev is shown in Figure 9b, and at a drill feed of f = 0.15 mm/rev is shown in Figure 9c.

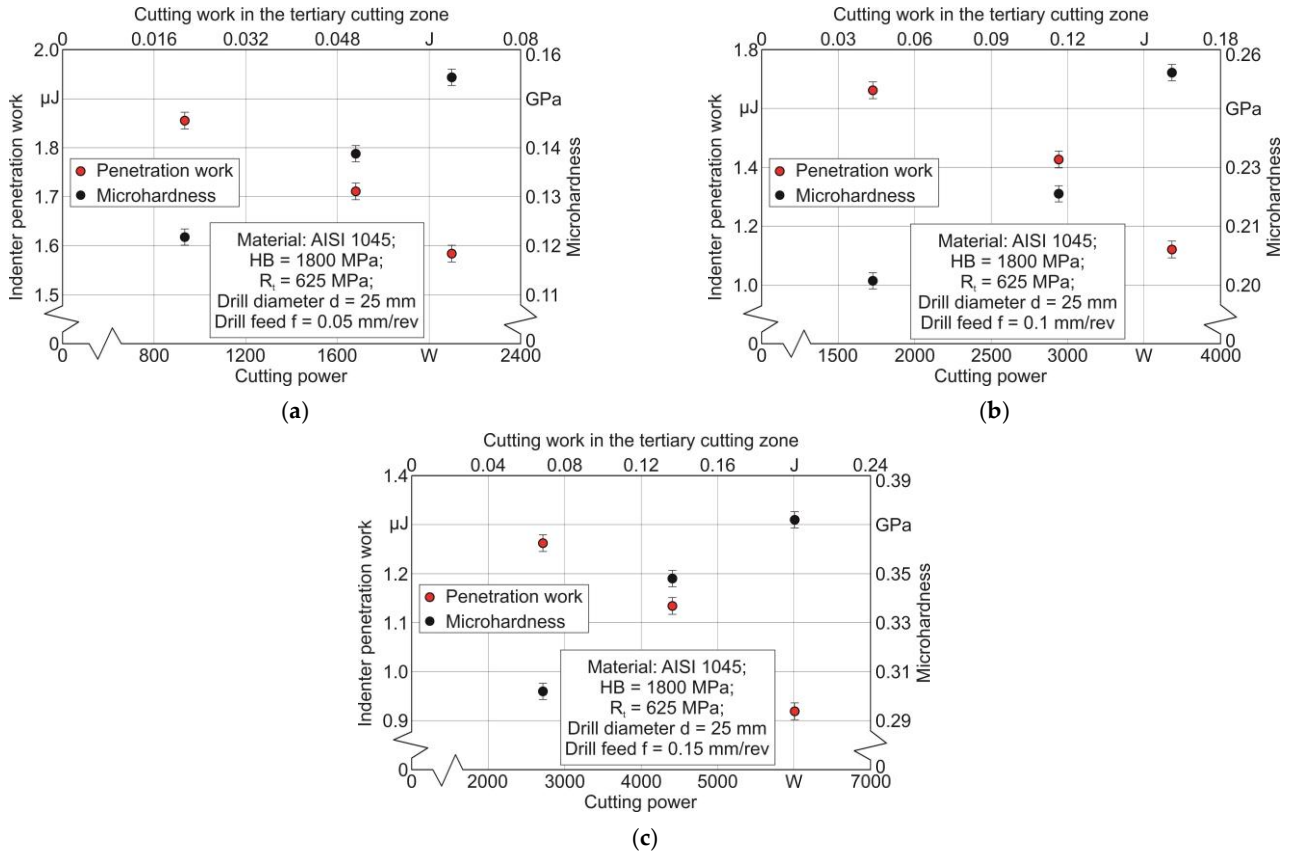

Figure 9. The coincidence of the indenter penetration work and microhardness with the cutting power and cutting work in the tertiary cutting zone: (**a**) at a drill feed of f = 0.05 mm/rev; (**b**) at a drill feed of f = 0.1 mm/rev; (**c**) at a drill feed of f = 0.15 mm/rev.

As increasing power P_C and work A_{dcf} are caused due to increasing cutting speed, the indenter penetration work W_{IN} increases monotonically for all studied values of drill feeds. At the same time, the microhardness of the machined subsurface layers decreases with increasing P_C and work A_{dcf} for all studied values of drill feed (see Figure 9).

Figure 10 shows the coincidence of the maximum indenter penetration depth with the total drilling power P_C and cutting work in the tertiary cutting zone A_{dcf}) at the different drill feeds indicated above. As these energy characteristics increase, the indenter penetration depth decreases.

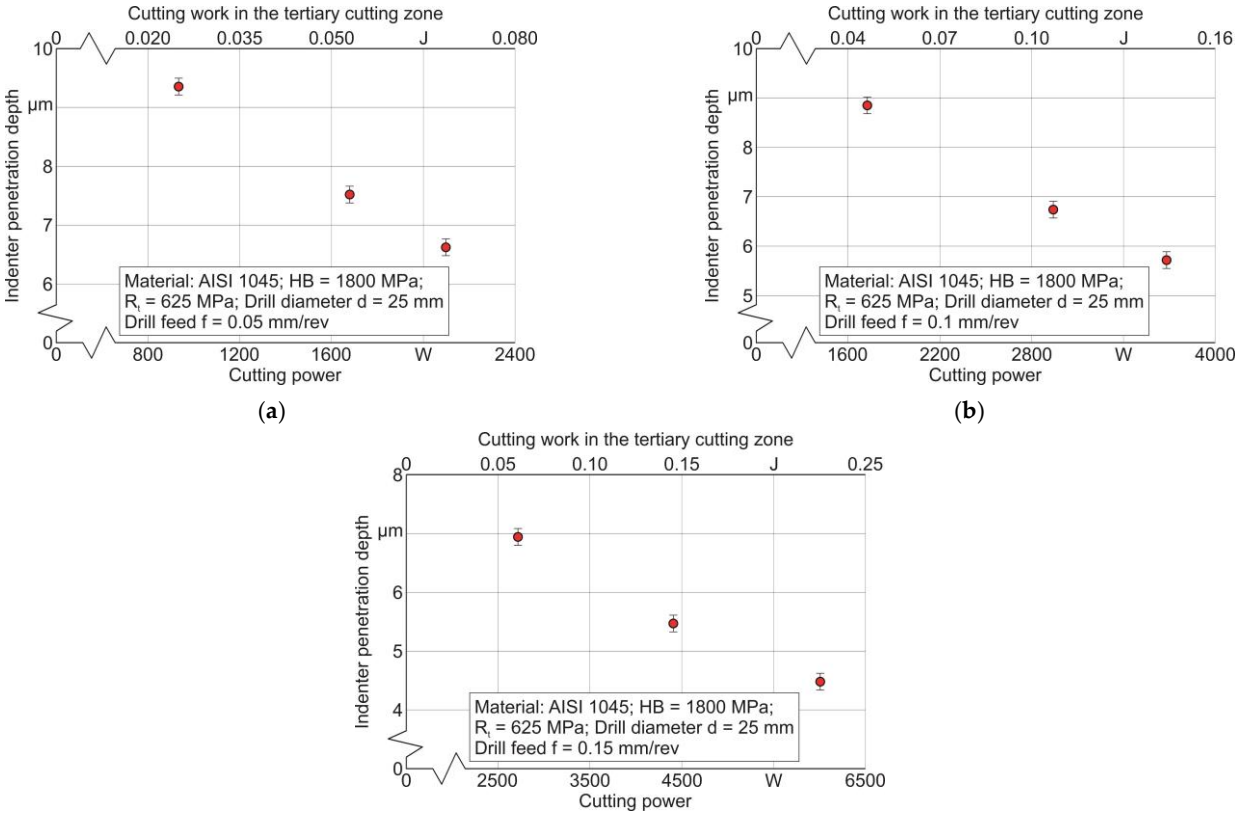

Figure 10. The coincidence of indenter penetration depth during sclerometry with the cutting power and cutting work in the tertiary cutting zone: (**a**) at the drill feed of f = 0.05 mm/rev; (**b**) at the drill feed of f = 0.1 mm/rev; (**c**) at the drill feed of f = 0.15 mm/rev.

The changes in the investigated mechanical characteristics shown in Figures 9 and 10 are explained by the hardening of the drill holes subsurface layers as a result of the cutting process [84,96]. Thus, an increase in the energy characteristics of the drilling process (power P_C and work A_{dcf}), expressed in the form of subsurface layers hardening, prevents the indenter's ability to penetrate these layers. Hence, the cutting process provides pumping a certain part of its energy into the drill holes subsurface layers, generating specific mechanical characteristics in these layers. In turn, the mechanical characteristics of subsurface layers significantly determine the service properties of parts manufactured by the cutting process, as well as their durability and serviceability. Thus, the coincidence of energy characteristics from the drilling process and mechanical characteristics discussed above allows for the required or specified service properties of manufactured parts to be provided by controlling the energy characteristics above.

6. Conclusions

The research object of the present study is to analyze the coincidence between the energy characteristics of the short hole drilling process and the mechanical characteristics of the drill holes' subsurface layers. The energy characteristics of the drilling process are the total drilling power and the cutting work in the tertiary cutting zone. The microhardness of drill holes subsurface layers and the total indenter penetration work, as well as the

maximum indenter penetration depth, were used as mechanical characteristics of the subsurface layers.

The cutting power was determined using the measured components of cutting forces. The cutting work in the tertiary cutting zone was calculated by numerical modeling of the short hole drilling process. The validity of the finite element model for the drilling process developed for this purpose was checked by comparing the measured and simulated values of the resulting cutting force. The difference between these values of cutting forces at nominal cutting speed V_C equal to 50 m/min ranged from 10.6 to 18.2% for the drill feed range from 0.05 mm/rev to 0.15 mm/rev. For the nominal cutting speed equal to 100 m/min, the deviation values ranged from 12.1% to 22.7%, and for the cutting speed equal to 150 m/min, from 18.6% to 26%, respectively.

The increase in the energy characteristics of the short hole drilling process causes an increase in the microhardness of the drill holes' subsurface layers. At the same time, this leads to a decrease in the total indenter penetration work and the maximum indenter penetration depth. The reason for this coincidence between the energy characteristics of the drilling process and the mechanical characteristics of the subsurface layers is the prevalence of the phenomenon of strain and strain rate hardening of these subsurface layers over their thermal softening.

The patterns of the identified coincidence between the energy characteristics of the short hole drilling process and the mechanical characteristics of the drill holes' subsurface layers ensure the possibility of controlling the performance properties of the machined parts using the studied drilling process.

Author Contributions: Conceptualization, M.S.; methodology, M.S.; software, M.S.; validation, M.S., L.H., and O.M.; formal analysis, M.S.; investigation, M.S., L.H., O.M. and N.B.; resources, M.S., O.M. and N.B.; data curation, M.S., L.H., and N.B.; writing—original draft preparation, M.S.; writing—review and editing, M.S.; visualization, M.S., L.H., and N.B.; project administration, M.S and O.M.; funding acquisition, M.S. All authors have read and agreed to the published version of the manuscript.

Funding: This study was funded by the German Research Foundation (DFG) in the project HE-1656/153-1, "Development of a Concept for Determining the Mechanical Properties of the Cutting Material in Machining".

Data Availability Statement: The original contributions presented in the study are included in the article, further inquiries can be directed to the corresponding author.

Acknowledgments: The authors would like to thank the German Research Foundation (DFG) for their support, which is highly appreciated.

Conflicts of Interest: The authors declare no conflicts of interest.

References

1. Guo, Y.; Saldana, C.; Compton, W.D.; Chandrasekar, S. Controlling deformation and microstructure on machined surfaces. *Acta Mater.* **2011**, *59*, 4538–4547. [CrossRef]
2. Sagapuram, D.; Udupa, A.; Viswanathan, K.; Mann, J.B.; M'Saoubi, R.; Sugihara, T.; Chandrasekar, S. On the Cutting of Metals: A Mechanics Viewpoint. *ASME J. Manuf. Sci. Eng.* **2020**, *142*, 110808. [CrossRef]
3. Davim, J.P. *Machining of Complex Sculptured Surfaces*; Springer: London, UK, 2012; 258p. [CrossRef]
4. Babichev, D.; Storchak, M. Synthesis of cylindrical gears with optimum rolling fatigue strength. *Prod. Eng. Res. Dev.* **2015**, *9*, 87–97. [CrossRef]
5. Bag, R.; Panda, A.; Sahoo, A.K.; Kumar, R. A Perspective Review on Surface Integrity and Its Machining Behavior of AISI 4340 Hardened Alloy Steel. *Mater. Today Proc.* **2019**, *18 Pt 7*, 3532–3538. [CrossRef]
6. Soori, M.; Arezoo, B. A Review in Machining-Induced Residual Stress. *J. New Technol. Mater.* **2022**, *12*, 64–83. Available online: https://hal.science/hal-03679993 (accessed on 19 April 2019).
7. Malakizadi, A.; Bertolini, R.; Ducobu, F.; Kilic, Z.M.; Magnanini, M.C.; Shokrani, A. Recent advances in modelling and simulation of surface integrity in machining—A review. *Procedia CIRP* **2022**, *115*, 232–240. [CrossRef]
8. Nagaraj, M.; Ezilarasan, C.; Kumar, A.J.P.; Velayudham, A. A review of machining characteristics in mechanical drilling of super alloy. *Int. J. Mech. Prod. Eng. Res. Dev.* **2018**, *8*, 579–588. [CrossRef]

9. Kanaev, A.T.; Ramazanova, Z.M.; Biizhanov, S.K. Study of plasma-hardened wheel steel using nanoindentation. Industrial laboratory. *Diagn. Mater.* **2020**, *86*, 56–60. (In Russian) [CrossRef]
10. Randall, N.X. The current state-of-the-art in scratch testing of coated systems. *Surf. Coat. Technol.* **2019**, *380*, 125092. [CrossRef]
11. Storchak, M. Mechanical Characteristics Generation in the Workpiece Subsurface Layers through Cutting. *Crystals* **2023**, *13*, 761. [CrossRef]
12. Komanduri, R. Machining and Grinding: A Historical Review of the Classical Papers. *Appl. Mech. Rev.* **1993**, *46*, 80–132. [CrossRef]
13. Davim, J.P. *Drilling Technology: Fundamentals and Recent Advances*; De Gruyter Oldenbourg: Boston, MA, USA, 2018; 205p, ISBN 978-3110478631.
14. Krishnaraj, V.; Zitoune, R.; Collombet, F. Comprehensive Review on Drilling of Multimaterial Stacks. *J. Mach. Form. Technol.* **2010**, *2*, 1–32.
15. Kheireddine, A.H.; Ammouri, A.H.; Lu, T.; Jawahir, I.S.; Hamade, R.F. An FEM Analysis with Experimental Validation to Study the Hardness of In-Process Cryogenically Cooled Drilled Holes in Mg AZ31b. *Procedia CIRP* **2013**, *8*, 588–593. [CrossRef]
16. Wegert, R.; Guski, V.; Schmauder, S.; Möhring, H.C. In-process approach for editing the subsurface properties during single-lip deep hole drilling using a sensor-integrated tool. *Prod. Eng. Res. Dev.* **2024**, *18*, 319–337. [CrossRef]
17. Sun, Z.; Geng, D.; Guo, H.; Zhang, Q.; Liu, Y.; Liu, L.; Jiang, X.; Zhang, D. Introducing transversal vibration in twist drilling: Material removal mechanisms and surface integrity. *J. Mater. Process. Technol.* **2024**, *325*, 118296. [CrossRef]
18. Strodick, S.; Schmidt, R.; Donnerbauer, K.; Rozo Vasquez, J.; Zabel, A.; Macias Barrientos, M.; Biermann, D.; Walther, F. Subsurface conditioning in BTA deep hole drilling for improved component performance. *Prod. Eng. Res. Dev.* **2024**, *18*, 299–317. [CrossRef]
19. Ren, X.; Liu, Z. Influence of cutting parameters on work hardening behavior of surface layer during turning superalloy Inconel 718. *Int. J. Adv. Manuf. Technol.* **2016**, *86*, 2319–2327. [CrossRef]
20. Garg, S.; Goyal, R.K. A Study of Surface Roughness in Drilling of AISI H11 Die Steel using Face Centered Design. *Int. J. Innov. Res. Sci. Technol.* **2015**, *1*, 464–474.
21. Lacombe, A.; Landon, Y.; Paredes, M.; Chirol, C.; Benaben, A. Influence of the Hole Surface Integrity on the Fatigue Strength of an Aluminium Drilled Part. In *Advances on Mechanics, Design Engineering and Manufacturing III. JCM 2020*; Roucoules, L., Paredes, M., Eynard, B., Morer Camo, P., Rizzi, C., Eds.; Lecture Notes in Mechanical Engineering; Springer: Cham, Switzerland, 2020. [CrossRef]
22. Farid, A.A.; Sharif, S.; Idris, M.H. Surface integrity study of high-speed drilling of Al–Si alloy using HSS drill. *Proc. Inst. Mech. Eng. Part B J. Eng. Manuf.* **2011**, *225*, 1001–1007. [CrossRef]
23. Barik, T.; Pal, K.; Parimita, S.; Sahoo, P.; Patra, K. Monitoring of hole surface integrity in drilling of bi-directional woven carbon fiber reinforced plastic composites. *Proc. Inst. Mech. Eng. Part C J. Mech. Eng. Sci.* **2020**, *234*, 2432–2458. [CrossRef]
24. Mendas, M.; Benayoun, S.; Miloud, M.H.; Zidane, I. Microhardness model based on geometrically necessary dislocations for heterogeneous material. *J. Mater. Res. Technol.* **2021**, *15*, 2792–2801. [CrossRef]
25. Ameri, A.A.H.; Elewa, N.N.; Ashraf, M.; Escobedo-Diaz, J.P. General methodology to estimate the dislocation density from microhardness measurements. *Mater. Charact.* **2017**, *131*, 324–330. [CrossRef]
26. Varote, N.; Joshi, S.S. Microstructural Analysis of Machined Surface Integrity in Drilling a Titanium Alloy. *J. Mater. Eng. Perform.* **2017**, *26*, 4391–4401. [CrossRef]
27. Haddag, B.; Yameogo, D.; Nouari, M.; Makich, H. Multi-Physics Analysis of Machining Ti-6Al-4V Alloy: Experimental Characterization and a New Material Behavior Modeling. *Metals* **2022**, *12*, 581. [CrossRef]
28. Wang, Z.-Y.; Ren, J.-X.; Zhou, J.-H.; Cai, J. Correlation analysis of microstructure evolution on microhardness and residual stress for cutting Ti-6Al-4V titanium alloy. *Proc. Inst. Mech. Eng. Part B J. Eng. Manuf.* **2023**, *237*, 885–898. [CrossRef]
29. Harun, S.; Burhanuddin, Y.; Ibrahim, G.A. The Effect of Cutting Parameters on Surface Roughness and Morphology of Ti-6Al-4V ELI Titanium Alloy during Turning with Actively Driven Rotary Tools. *J. Manuf. Mater. Process.* **2022**, *6*, 105. [CrossRef]
30. Hussein, R.; Sadek, A.; Elbestawi, M.A.; Attia, M.H. Surface and microstructure characterization of low-frequency vibration-assisted drilling of Ti6Al4V. *Int. J. Adv. Manuf. Technol.* **2019**, *103*, 1443–1457. [CrossRef]
31. Hou, G.; Li, A. Effect of Surface Micro-Hardness Change in Multistep Machining on Friction and Wear Characteristics of Titanium Alloy. *Appl. Sci.* **2021**, *11*, 7471. [CrossRef]
32. Rangasamy, N.; Rakurty, C.S.; Balaji, A.K. A Multiscale Study on Machining Induced Surface Integrity in Ti-6Al-4V Alloy. *Procedia CIRP* **2022**, *108*, 787–792. [CrossRef]
33. Rodriguez, I.; Arrazola, P.J.; Cuesta, M.; Sterle, L.; Pušavec, F. Improving surface integrity when drilling CFRPs and Ti-6Al-4V using sustainable lubricated liquid carbon dioxide. *Chin. J. Aeronaut.* **2023**, *36*, 129–146. [CrossRef]
34. Murad, M.N.; Sharif, S.; Rahim, E.A.; Rival, R. Effect of Drill Point Angle on Surface Integrity when Drilling Titanium Alloy. *In Adv. Mater. Res.* **2013**, *845*, 966–970. [CrossRef]
35. Lotfi, M.; Farid, A.A.; Akbari, J.; Sharif, S.; Mohruni, A.S. Evaluation of surface integrity when drilling Inconel 718 through experimental measurement and finite element analysis. *Int. J. Adv. Manuf. Technol.* **2022**, *119*, 4237–4248. [CrossRef]
36. Dutilh, V.; Dessein, G.; Alexis, J.; Perrin, G. Links Between Machining Parameters and Surface Integrity in Drilling Ni-Superalloy. *Adv. Mater. Res.* **2010**, *112*, 171–178. [CrossRef]
37. Xu, D.; Ding, L.; Liu, Y.; Zhou, J.; Liao, Z. Investigation of the Influence of Tool Rake Angles on Machining of Inconel 718. *J. Manuf. Mater. Process.* **2021**, *5*, 100. [CrossRef]

38. Rahim, E.A.; Sasahara, H. An Analysis of Surface Integrity when Drilling Inconel 718 Using Palm Oil and Synthetic Ester under MQL Condition. *Mach. Sci. Technol.* **2011**, *15*, 76–90. [CrossRef]
39. Karabulut, Y.; Kaynak, Y. Drilling process and resulting surface properties of Inconel 718 alloy fabricated by Selective Laser Melting Additive Manufacturing. *Procedia CIRP* **2020**, *87*, 355–359. [CrossRef]
40. Girinon, M.; Valiorgue, F.; Rech, J.; Feulvarch, E. Development of a Procedure to Characterize Residual Stresses Induced by Drilling. *Procedia CIRP* **2016**, *45*, 79–82. [CrossRef]
41. Nobre, J.P.; Outeiro, J.C. Evaluating Residual Stresses Induced by Drilling of Ti-6Al-4V Alloy by Using an Experimental-numerical Methodology. *Procedia CIRP* **2015**, *31*, 215–220. [CrossRef]
42. Rasti, A.; Sadeghi, M.H.; Farshi, S.S. An analytical study on residual stresses in drilling of hardened steel. *Int. J. Adv. Manuf. Technol.* **2018**, *99*, 2389–2405. [CrossRef]
43. Leveille, T.; Valiorgue, F.; Dumas, M.; Masciantonio, U.; Brosse, A.; Karaouni, H.; Rech, J. 3D numerical modelling of residual stresses induced by reaming. *J. Manuf. Process.* **2024**, *113*, 47–60. [CrossRef]
44. Wu, R.; Huang, S.; Zhang, W.; Zhu, M.; Zheng, Z.; Li, T.; Xue, H. An improved grey wolf optimizer for minimizing drilling deformation and residual stress in AA2024 sheet. *Int. J. Adv. Manuf. Technol.* **2024**, *130*, 4443–4458. [CrossRef]
45. Pharr, G.M. Recent advances in small-scale mechanical property measurement by nanoindentation. *Curr. Opin. Solid State Mater. Sci.* **2015**, *19*, 315–316. [CrossRef]
46. Fischer-Cripps, A.C. Critical review of analysis and interpretation of nanoindentation test data. *Surf. Coat. Technol.* **2006**, *200*, 4153–4165. [CrossRef]
47. Wredenberg, F.; Larsson, P.-L. Scratch testing of metals and polymers: Experiments and numerics. *Wear* **2009**, *266*, 76–83. [CrossRef]
48. Kolawole, O.; Ispas, I. Evaluation of geomechanical properties via scratch tests: Where are we and where do we go from here? *SN Appl. Sci.* **2020**, *2*, 1633. [CrossRef]
49. Fischer-Cripps, A.C. *Nanoindentation*, 2nd ed.; Springer: Berlin/Heidelberg, Germany, 2011; 276p. [CrossRef]
50. Atkins, A.G.; Tabor, D. Plastic Indentation in Metals with Cones. *J. Mech. Phys. Solids* **1965**, *13*, 149–164. [CrossRef]
51. Doerner, M.; Nix, W. A method for interpreting the data from depth-sensing indentation instruments. *J. Mater. Res.* **1986**, *1*, 601–609. [CrossRef]
52. Oliver, W.C.; Pharr, G.M. An improved technique for determining hardness and elastic modulus using load and displacement sensing indentation experiments. *J. Mater. Res.* **1992**, *7*, 1564–1583. [CrossRef]
53. Zivic, F.; Babic, M.; Adamovic, D.; Mitrovic, S.; Todorovic, P.; Favaro, G.; Pantić, M. Influence of the surface roughness on adhesion of chrome coatings on alloy tool steel x165crmov12. *J. Balk. Tribol. Assoc.* **2012**, *18*, 228–237.
54. Bull, S.J. Failure modes in scratch adhesion testing. *Surf. Coat. Technol.* **1991**, *50*, 25–32. [CrossRef]
55. Lin, C.K.; Berndt, C.C. Measurement and analysis of adhesion strength for thermally sprayed coatings. *J. Therm. Spray Technol.* **1994**, *3*, 75–104. [CrossRef]
56. Yildiz, F.; Asaran, A. Multi-pass scratch test behavior of modified layer formed during plasma nitriding. *Tribol. Int.* **2010**, *43*, 1472–1478. [CrossRef]
57. Storchak, M.; Zakiev, I.; Träris, L. Mechanical properties of subsurface layers in the machining of the titanium alloy $Ti_{10}V_2Fe_3Al$. *J. Mech. Sci. Technol.* **2018**, *32*, 315–322. [CrossRef]
58. Sousa, F.J.P.; Tridapalli, D.; Pereira, M.; Flesch, C.A.; Alarcon, O.E. Evaluation of measurement uncertainties for a scratching tester. *Measurement* **2006**, *39*, 594–604. [CrossRef]
59. Fritz, R.; Kiener, D. Development and application of a heated in-situ SEM micro-testing device. *Measurement* **2017**, *110*, 356–366. [CrossRef]
60. Sivaram, S.; Jayasinghe, J.A.S.C.; Bandara, C.S. Qualitative Study on Pile-up Effect on Hardness Test by Nano-Indentation. *Eng. J. Inst. Eng.* **2021**, *54*, 47–55. [CrossRef]
61. Farayibi, P.K.; Hankel, J.; van gen Hassend, F.; Blüm, M.; Weber, S.; Röttger, A. Tribological characteristics of sintered martensitic stainless steels by nano-scratch and nanoindentation tests. *Wear* **2023**, *512–513*, 204547. [CrossRef]
62. Li, Z.; Herrmann, K.; Pohlenz, F. A comparative approach for calibration of the depth measuring system in a nanoindentation instrument. *Measurement* **2006**, *39*, 547–552. [CrossRef]
63. Peng, G.; Xu, F.; Chen, J.; Hu, Y.; Wang, H.; Zhang, T. A cost-effective voice coil motor-based portable micro-indentation device for in situ testing. *Measurement* **2020**, *165*, 108105. [CrossRef]
64. Ding, K.; Zhang, Y.; Birnbaum, A.J.; Michopoulos, J.G.; McDowell, D.L.; Zhu, T. Strain gradient plasticity modeling of nanoindentation of additively manufactured stainless steel. *Extrem. Mech. Lett.* **2021**, *49*, 101503. [CrossRef]
65. Vargas, A.L.M.; Blando, E.; Hübler, R. Elasto—Plastic materials behavior evaluation according to different models applied in indentation hardness tests. *Measurement* **2019**, *139*, 134–139. [CrossRef]
66. Kang, J.J.; Becker, A.A.; Wen, W.; Sun, W. Extracting elastic-plastic properties from experimental loading-unloading indentation curves using different optimization techniques. *Int. J. Mech. Sci.* **2018**, *144*, 102–109. [CrossRef]
67. Tsybenko, H.; Farzam, F.; Dehm, G.; Brinckmann, S. Scratch hardness at a small scale: Experimental methods and correlation to nanoindentation hardness. *Tribol. Int.* **2021**, *163*, 107168. [CrossRef]

68. England, J.; Uddin, M.J.; Ramirez-Cedillo, E.; Karunarathne, D.; Nasrazadani, S.; Golden, T.D.; Siller, H.R. Nanoindentation Hardness and Corrosion Studies of Additively Manufactured 316L Stainless Steel. *J. Mater. Eng. Perform.* **2022**, *31*, 6795–6805. [CrossRef]
69. Moon, J.; Kim, S.; Jang, J.; Lee, J.; Lee, C. Orowan strengthening effect on the nanoindentation hardness of the ferrite matrix in microalloyed steels. *Mater. Sci. Eng. A* **2008**, *487*, 552–557. [CrossRef]
70. Li, C.; Zhao, H.; Sun, L.; Yu, X. In situ nanoindentation method for characterizing tensile properties of AISI 1045 steel based on mesomechanical analysis. *Adv. Mech. Eng.* **2019**, *11*, 1687814019862919. [CrossRef]
71. Paul, V.; Ameyama, K.; Ota-Kawabata, M.; Ohmura, T. Evaluation of Deformation and Fracture Behavior in 304L Austenitic Steel Harmonic Structures through Nanoindentation. *Steel Res. Int.* **2023**, *94*, 2200354. [CrossRef]
72. Zhou, G.; Guo, J.; Zhao, J.; Tang, Q.; Hu, Z. Nanoindentation Properties of 18CrNiMo7-6 Steel after Carburizing and Quenching Determined by Continuous Stiffness Measurement Method. *Metals* **2020**, *10*, 125. [CrossRef]
73. Dean, J.; Aldrich-Smith, G.; Clyne, T.W. Use of nanoindentation to measure residual stresses in surface layers. *Acta Mater.* **2011**, *59*, 2749–2761. [CrossRef]
74. Wang, H.; Zhu, L.; Xu, B. *Residual Stresses and Nanoindentation Testing of Films and Coatings*; Springer Nature Singapore Pte Ltd.: Singapore; Science Press: Beijing, China, 2018; 207p, ISBN 978-981-10-7840-8. [CrossRef]
75. Zhang, W.; Wang, X.; Hu, Y.; Wang, S. Predictive modelling of microstructure changes, micro-hardness and residual stress in machining of 304 austenitic stainless steel. *Int. J. Mach. Tools Manuf.* **2018**, *130–131*, 36–48. [CrossRef]
76. Fan, P.; Katiyar, N.K.; Zhou, X.; Goel, S. Uniaxial pulling and nano-scratching of a newly synthesised high entropy alloy. *APL Mater.* **2022**, *10*, 111118. [CrossRef]
77. Pratap, A.; Divse, V.; Goel, S.; Joshi, S.S. Understanding the surface generation mechanism during micro-scratching of Ti-6Al-4V. *J. Manuf. Process.* **2022**, *82*, 543–558. [CrossRef]
78. Liu, H.; Xu, X.; Zhang, J.; Liu, Z.; He, Y.; Zhao, W.; Liu, Z. The state of the art for numerical simulations of the effect of the microstructure and its evolution in the metal-cutting processes. *Int. J. Mach. Tools Manuf.* **2022**, *177*, 103890. [CrossRef]
79. Bezyazychnyy, V.F.; Prokofev, M.A.; Vinogradova, N.V. Research of the Influence of Technological Machining Conditions on the Accumulation of Latent Energy Deformation in the surface Parts. *Bull. PNIPU Aerosp. Eng.* **2015**, *43*, 131–144. [CrossRef]
80. Yamamoto, M.; Tanaka, M.; Furukimi, O. Hardness–Deformation Energy Relationship in Metals and Alloys: A Comparative Evaluation Based on Nanoindentation Testing and Thermodynamic Consideration. *Materials* **2021**, *14*, 7217. [CrossRef] [PubMed]
81. Storchak, M.; Stehle, T.; Möhring, H.-C. Numerical Modeling of Cutting Characteristics during Short Hole Drilling: Modeling of Kinetic Characteristics. *J. Manuf. Mater. Process.* **2023**, *7*, 195. [CrossRef]
82. Material Property Data. Available online: http://www.matweb.com (accessed on 19 April 2019).
83. Storchak, M.; Stehle, T.; Möhring, H.-C. Determination of thermal material properties for the numerical simulation of cutting processes. *Int. J. Adv. Manuf.* **2021**, *118*, 1941–1956. [CrossRef]
84. Oxley, P.L.B. Development and Application of a Predictive Machining Theory. *Mach. Sci. Technol.* **1998**, *2*, 165–189. [CrossRef]
85. Heisel, U.; Kushner, V.; Storchak, M. Effect of machining conditions on specific tangential forces. *Prod. Eng.* **2012**, *6*, 621–629. [CrossRef]
86. Tsekhanov, J.; Storchak, M. Development of analytical model for orthogonal cutting. *Prod. Eng. Res. Dev.* **2015**, *9*, 247–255. [CrossRef]
87. Heisel, U.; Krivoruchko, D.V.; Zaloha, W.A.; Storchak, M.; Stehle, T. Thermomechanical material models in the modeling of cutting processes. *ZWF Z. Fuer Wirtsch. Fabr.* **2009**, *104*, 482–491. [CrossRef]
88. Storchak, M.; Jiang, L.; Xu, Y.; Li, X. Finite element modeling for the cutting process of the titanium alloy $Ti_{10}V_2Fe_3Al$. *Prod. Eng. Res. Dev.* **2016**, *10*, 509–517. [CrossRef]
89. Johnson, G.R.; Cook, W.H. A constitutive model and data for metals subjected to large strains, high strain and high temperatures. In Proceedings of the 7th International Symposium on Ballistics, The Hague, The Netherlands, 19–21 April 1983; pp. 541–547.
90. Heisel, U.; Krivoruchko, D.V.; Zaloha, W.A.; Storchak, M.; Stehle, T. Thermomechanical exchange effects in machining. *ZWF Z. Fuer Wirtsch. Fabr.* **2009**, *104*, 263–272. [CrossRef]
91. Storchak, M.; Möhring, H.-C.; Stehle, T. Improving the friction model for the simulation of cutting processes. *Tribol. Int.* **2022**, *167*, 107376. [CrossRef]
92. Fluhrer, J. *Deform-User Manual Deform V12.0*; SFTC: Columbus, OH, USA, 2019.
93. Heisel, U.; Krivoruchko, D.V.; Zaloha, W.A.; Storchak, M.; Stehle, T. Breakage models for the modeling of cutting processes. *ZWF Z. Fuer Wirtsch. Fabr.* **2009**, *104*, 330–339. [CrossRef]
94. Storchak, M.; Kushner, V.; Möhring, H.-C.; Stehle, T. Refinement of temperature determination in cutting zones. *J. Mech. Sci. Technol.* **2021**, *35*, 3659–3673. [CrossRef]
95. Kushner, V.; Storchak, M. Determining mechanical characteristics of material resistance to deformation in machining. *Prod. Eng. Res. Dev.* **2014**, *8*, 679–688. [CrossRef]

96. Kushner, V.; Storchak, M. Determination of Material Resistance Characteristics in Cutting. *Procedia CIRP* **2017**, *58*, 293–298. [CrossRef]
97. Heisel, U.; Storchak, M.; Krivoruchko, D.V. Thermal effects in orthogonal cutting. *Prod. Eng. Res. Dev.* **2013**, *7*, 203–211. [CrossRef]

Disclaimer/Publisher's Note: The statements, opinions and data contained in all publications are solely those of the individual author(s) and contributor(s) and not of MDPI and/or the editor(s). MDPI and/or the editor(s) disclaim responsibility for any injury to people or property resulting from any ideas, methods, instructions or products referred to in the content.